Conference paper

Filip Mamon, Radek Fajgar, Vera Jandova, Eva Koci, Ivo Jakubec, Alexander Zhigunov, Tatjana Brovdyova and Snejana Bakardjieva*

TiO_2 microrods with stacked 3D nanovoids for photoelectrochemical water splitting

https://doi.org/10.1515/pac-2018-1116

Abstract: This paper reports an original nonstandard green concept to obtain TiO_2 microrods with polyhedral densely stacked 3D nanovoids prepared via the heat treatment of a hydrogen titanate. The intermediate hydrogen titanate was synthesized by a solid-liquid-solid (SLS) route from an ammonia-saturated aqueous solution of $TiOSO_4$ at 0 °C. The effect of the postgrowth thermal annealing procedure to remove ice (water) and the proposed mechanism to explain the underlying transitions from the intermediate precursor to nanostructured TiO_2 microrods with stacked 3D nanovoids were investigated. The small-angle X-ray scattering (SAXS) analysis indicates that at temperatures above 500 °C, the release of confined ice (water) takes place, which leads to the creation of self-assembled polyhedral nanovoids open to the surface. Their size ranges from 5 to 78 nm in both length and width, with a depth of ~3.88 nm. The first use of these stacked 1D TiO_2 microrods as the working electrode in a photoelectrochemical (PEC) cell for water splitting is demonstrated. The estimated value of ζ-potential depends on both annealing temperature and crystallite size. Anatase sample 1D TiO/800 with ζ-potential (–29.1) mV and average crystallite size ~68 nm was observed to be highly stable in aqueous suspension. The SLS method yields low-cost 1D TiO_2 materials possessing high photoreactivity with water. The PEC measurements indicate that three-dimensional hollow structures with a controlled geometry via patterned 1D TiO_2 surface are promising materials for hydrogen generation from water splitting.

Keywords: nanovoids; photoelectrochemistry; SSC-2018; TiO_2 microrods; water splitting.

Introduction

Over the past decade, one-dimensional (1D) TiO_2 nanostructures have attracted attention because of their unique optical and electronic properties, for instance, a large surface area and a directed electron path [1, 2]. Due to the increasing need of clean energy production, a significant effort has been made to exploit the properties of 1D TiO_2 materials for applications such as photovoltaics and related solar-harvesting devices. Semiconductor photoelectrodes based on TiO_2, which has conduction and valence band-edge positions

Article note: A collection of invited papers based on presentations at the 13th International Conference on Solid State Chemistry (SSC-2018), Pardubice, Czech Republic, September 16–21, 2018.

***Corresponding author: Snejana Bakardjieva,** Institute of Inorganic Chemistry of the Czech Academy of Sciences, 205 68 Rez, Czech Republic, e-mail: snejana@iic.cas.cz

Filip Mamon, Eva Koci and Ivo Jakubec: Institute of Inorganic Chemistry of the Czech Academy of Sciences, 205 68 Rez, Czech Republic

Radek Fajgar and Vera Jandova: Institute of Chemical Process and Fundamentals of the Czech Academy of Sciences, Rozvojova 2/135, 165 02 Prague, Czech Republic

Alexander Zhigunov: Institute of Macromolecular Chemistry of the Czech Academy of Sciences, Heyrovskeho nam.1888/2, 162 00 Prague, Czech Republic

Tatjana Brovdyova: Faculty of Mechanical Engineering, Jan Evangelista Purkyne University, Pasteurova 3334/7, 400 96 Usti nad Labem, Czech Republic

enabling both the hydrogen and oxygen evolution reaction (HER/OER), are highly desired to increase the simplicity of the overall water splitting device architecture [3]. The splitting of water molecules with sunlight to produce molecular hydrogen (and oxygen) is one of the most benign forms of energy production since water and sunlight are both vastly abundant. Solar-harvesting devices such as PEC cells [4] can be an important source of sustainable alternative energy for the burgeoning hydrogen economy. The first study of PEC water splitting on TiO_2 was reported in 1972 by Fujishima and Honda [5], who showed that the TiO_2 photoanode exhibits outstanding photoelectrochemical (PEC) properties that may be utilized for the conversion of solar energy into chemical energy. In 1978, Nozik [6] predicted that it will be possible to optimize the basic reaction of a photoelectrosynthetic cell by means of micro- or nanoscale particles that can split water under illumination. The above mentioned remarkable discoveries resulted in an increased interest in TiO_2-based materials. The details surrounding the direct photocatalytic splitting of water have been the subject of thousands of papers over the past four decades, with many being optimistic [7–17]. The most critical issue in solar-hydrogen generation is the development of a high-performance photoelectrode. One of the most important steps during the PEC process is achieving a photoelectrode with a high photoreactivity towards water on one hand and a resistance to photocorrosion in aqueous environments, stability and low processing costs on the other hand.

Nowotny et al. [18] identified six basic reactions involved in PEC solar-hydrogen generation when a single photoelectrode is applied: (1) photoionization over the band gap, (2) charge separation, (3) the reaction between water and electron holes at the surface of the photoanode, (4) the transport of hydrogen ions from the photoanode to the cathode through the liquid electrolyte, (5) the transport of electrons to the cathode through the external circuit and (6) the reaction between electrons and hydrogen ions at the cathode. The reaction between water and electron holes at the surface of the photoanode is expressed by

$$H_2O + 2h^+ \rightarrow 2H^+ + \frac{1}{2}O_2 \tag{1}$$

and is the PEC major reaction. It has also been documented [18] that efficient water decomposition must be considered in terms of the active surface sites available on the photoelectrode. These sites enable the formation of an active complex between TiO_2 and water, leading to the effective splitting of water into oxygen and hydrogen via the following reaction

$$2H_2O \rightarrow 2H_2(g) + O_2 \tag{2}$$

Therefore, the photoreactivity of TiO_2 towards water is related to both the collective properties (electronic structure, flat band potential and charge transport kinetics within the PEC reaction) and local factors in the TiO_2 structure (for instance, intrinsic point defects). Nanostructured TiO_2 materials with point defects can increase the quantum efficiency for water splitting by reducing the number of recombination states through decreasing the diffusion distance for the minority carrier. In addition, the directions of light absorption and charge carrier collection can be decoupled through planar 1D geometries [19, 20].

Here, novel nanostructures with densely stacked nanocavities inside a 1D morphology of TiO_2 have been prepared, which present excellent photocatalytic and electrochemical properties. Recently, the photocatalytic activity of 1D bicrystalline nanoribbons with alternating structures of TiO_2(B) and anatase was observed [21] under visible-light irradiation due to the formation of nanocavities inside the TiO_2 nanocrystals. The research revealed that the TiO_2(B) with nanocavities exhibited a narrow band gap and an improved absorption coefficient in the UV region. An enhanced optical absorption induced by dense nanovoids inside titania nanorods was also reported by Han et al. [22]. The molar absorption coefficient of TiO_2 nanorods with nanovoids (when the incident light wavelength was below 385 nm. close to 3.2 eV, the band gap of anatase TiO_2) was found to be approximately 25 % higher than that of TiO_2 without nanovoids. An easy method to synthesize nanovoid-structured TiO_2 microcrystals via a sol-gel route using titanium isopropoxide as a precursor was published by Usseglio et al. [23]. Their combined IR, Raman and TEM studies indicated that the nanovoids were formed during the thermal treatment at 773 K in air by the partial oxidation products (hydrogen

carbonates, adsorbed carbon dioxide, and residual OR groups) of the organic part of the precursor. The nanovoid-structured TiO_2 microcrystals were found to be active in the photodegradation of methylene blue but with a substantially lower efficiency than that of the commercial P25 TiO_2 photocatalyst due to its significantly lower surface area.

Our group recently reported a new preparation method (herein, we name it solid-liquid-solid, SLS) for the synthesis of 1D TiO_2 microrods (MRs) in aqueous media by starting with hydrated titanyl sulfate crystals ($TiOSO_4 \cdot 2H_2O$). The method is based on the extraction of sulfate ions from the $TiOSO_4$ crystals and their replacement with hydroxyl groups from the aqueous ammonia solution, leaving the Ti – O framework intact [24]. However, no attention was paid to the nanovoid phenomenon. In the present work, we turn our attention from the chemical properties of the studied materials to their structure and morphology. We are concerned with the nanovoid phenomenon governed by the evaporation of ice (water) and find that the as-created dense 3D nanocavities significantly enhance the electrochemical properties of TiO_2, thereby providing a new approach to increase the reactivity of 1D TiO_2 MRs for use in PEC cells for water splitting.

The chemical and morphological characteristics of the 1D TiO_2 MRs were studied by X-ray powder diffraction (XRD) and electron microscopy (SEM/EDS and HRTEM/SAED). X-ray photoelectron spectroscopy (XPS) was carried out to obtain information about the chemical and electronic state of the elements. The SAXS analysis was performed to obtain information about the depth of the nanovoids. Raman scattering was employed to investigate the evolution of the anatase phase in the 1D TiO_2 MRs during annealing. The stability of as-prepared samples was estimated by zeta potential (ζ) measurements. The UV-Vis analysis and the corresponding band-gap extraction were also evaluated. The splitting of water and evolution of hydrogen were performed in the electrochemical cell composed of three compartments (for working, counter and standard saturated Ag/AgCl electrodes), and information from the cyclic voltammetry experiment was also acquired.

Materials and methods

Materials

Titanium (IV) oxysulfate ($TiOSO_4 \cdot 2H_2O$, min 29 % Ti as TiO_2, Sigma-Aldrich, spol. s.r.o., Prague, Czech Republic) was served as a titanium precursor. Aqueous solution of ammonia (NH_3, solution purum p.a., 25–29 %, Fisher Scientific, spol. s.r.o., Pardubice Czech Republic) was used for chemical precipitation. Photoelectrochemical testing was performed in sodium sulfate ($Na_2SO_4 \geq 99$ %, Merck, Darmstadt, Germany,) solution.

Synthesis of 1D TiO_2 MRs

The 1D TiO_2 samples were synthesized as described in previous publication [24]. Briefly, a total of 100 mL of cooled distilled water was mixed with 50 g of ice, and 5 mL of aqueous ammonia. After adding 4.80 g of $TiOSO_4 \cdot 2H_2O$, the suspension had a temperature of 0 °C and pH 9. While the mixture was magnetically stirred for 4 h at pH 9, its temperature rose to room temperature (RT). Then the suspension was decanted twice, the solid precursor was filtered off and dried at RT. The intermediate solid precursor named 1D TiO was annealed in air at 500, 650, 800 and 950 °C for 1 h and four new samples denoted as 1D TiO/500, 1D TiO/650, 1D TiO/800 and 1D TiO/950 were safely isolated.

Changes in temperature were found to affect the transformation of intermediate amorphous precursor 1D TiO into aligned arrays of 1D MRs composed of TiO_2 nanocrystals (NCs). During this step, nanovoids with sharp polyhedral shape are formed inside annealed 1D TiO_2 MRs.

Characterization methods

X-ray powder diffraction

Diffraction patterns were collected using a PANalytical XPert PRO diffractometer equipped with a conventional X-ray tube ($Cu_{K\alpha}$ 40 kV, 30 mA, line focus) in transmission mode. An elliptic focusing mirror, a divergence slit 0.5°, an anti-scatter slit 0.5° and a Soller slit of 0.02 rad were used in the primary beam. A fast linear position sensitive detector PIXcel with an anti-scatter shield and a Soller slit of 0.02 rad were used in the diffracted beam. All patterns were collected in 2 theta (2θ) range of 18–88° with step of 0.013° and 400 s/step dwelling time, producing a scan of about 2.5 h. Qualitative analysis was performed with the HighScore-Plus software package (PANalytical, The Netherlands, version 3.0e), the DiffracPlus software package (Bruker AXS, Germany, version 8.0) and the JCPDS PDF database [25]. For quantitative phase analysis, DiffracPlus Topas (Bruker AXS, Germany, version 4.2) was used with structural models based on the ICSD database. This program allows the estimation of the weight fractions of crystalline phases by means of the Rietveld refinement procedure. The estimation of the size of crystallites was performed on the basis of the Scherrer formula [26] as implemented within the DiffracPlus Topas software.

Electron microscopy

The morphology of the powdered samples placed on the carbon tape was investigated using a scanning electron microscope (SEM) Philips XL30CP. Measurements were carried out in high vacuum mode (with secondary electrons detector) at accelerating voltage of 25 kV. The samples were observed without coating by the conductive layer to study their original texture. Transmission electron microscopy (TEM) was carried out on a JEOL JEM 3010 microscope operated at 300 kV (LaB_6 cathode, point resolution 1.7 Å) with an Oxford Instruments Energy Dispersive X-ray (EDS) detector attached. Images were recorded on a CCD camera with resolution of 1024×1024 pixels using the Digital Micrograph software package. EDS analyses were acquired and treated in the INCA software package. Electron diffraction patterns were evaluated using the Process Diffraction software package [27].

Thermal analysis

Thermogravimetry (TG) and differential thermal analysis (DTA) were performed with the apparatus SetSys Evolution (SETARAM). TA measurements of prepared samples were performed in a crucible made of α-Al_2O_3 in argon flow (60 mL min^{-1}) at atmospheric pressure in temperature range from room temperature (RT) to 1000 °C with heating rate of 5 °C min^{-1}. The dried fine powder (20–25 mg) of 1D TiO sample was measured.

Small-angle X-ray scattering (SAXS)

SAXS experiments were performed using a pinhole camera (modified Molecular Metrology System, Rigaku, Japan) attached to a microfocused X-ray beam generator (Rigaku MicroMax 003) operating at 50 kV and 0.6 mA (30 W). The camera was equipped with a vacuum version of Pilatus 300K hybrid-pixel detector (Dectris). Two experimental setups were used to cover the q range of 0.004–0.5 $Å^{-1}$. Scattering vector, q, is defined as: $q = (4\pi/\lambda)\sin 2\theta$, where λ is the wavelength and 2θ is the scattering angle. Calibration of primary beam position and sample-to-detector distances was performed using AgBehenate sample.

X-ray photoelectron spectroscopy

X-ray photoelectron spectra (XPS) were measured by Kratos ESCA 3400 furnished with a polychromatic Mg X-ray source of Mg Kα radiation (energy: 1253.4 eV). The base pressure was kept at 5.0×10^{-7} Pa.

The spectra were fitted using a Gaussian–Lorentzian line shape, Shirley background subtraction and a damped non-linear least square procedure. Survey spectra between 0 and 1000 eV were collected and more detailed spectra were taken over Ti 2p, O 1s, and C 1s regions. The samples were sputtered with Ar^+ ions at 1 kV with current of 10 μA for 90 s to remove superficial layers. Spectra were calibrated to C 1s line centered at 284.8 eV.

Raman spectroscopy

Raman spectra were collected by a Nicolet Almega XR dispersive spectrometer equipped with Olympus BX-51 microscope. Two hundred fifty-six expositions with resolution 2 cm^{-1} were taken using excitation wavelength 473 nm with energy 5 mW.

Zeta potential determinations (ζ-potential)

TiO_2 samples (0.5 mg) were dispersed in a distilled deionized water (10 mL) using ultrasound bath for 10 min. The (ζ) measurements were performed in a BI-SCP cells (10 mm optical path) using a HeNe laser beam 633 nm (NanoBrook Omni, Brookhaven Instruments Corp.). The measurements were repeated five times to check their reproducibility.

UV-Vis diffuse reflectance spectroscopy

The method of UV-Vis diffuse reflectance spectroscopy was employed to estimate band-gap energies of the TiO_2 samples. UV-Vis spectroscopy was carried out using a double beam Shimadzu spectrophotometer UV 1800. Reflectance spectra of the solid samples were measured in the range 190–550 nm using a PTFE as a standard. Kubelka-Munk transformation was then applied and Tauc plots were used to calculate the band-gap energy E_{bg} by the extrapolation of the linear part of $[F(R_\infty)hv]^{1/2}$ vs. energy dependency.

FTIR

The FTIR measurements in transmission mode were performed using Thermo Scientific Nicolet NEXUS 670 FT-IR. The samples were analysed in KBr pellets. The amount of the sample for the analysis was ranging from 1 mg/300 mg KBr. The acquisition of the spectra comprised 64 scans in the range of 4000–400 cm^{-1}, resolution being 4 cm^{-1}. The spectra were processed in OMNIC software package 8.3 [OMNIC Software Suite, version 8.3, © 1992–2011, Thermo Fisher Scientific, Inc., Waltham, MA, USA].

Water splitting experiment

The splitting of water and evolution of hydrogen were performed in the electrochemical cell composed of three compartments (for working, counter and standard saturated Ag/AgCl electrodes) filled with an electrolyte and separated by a semi-permeable membranes made of sintered glass. Sodium sulfate (Na_2SO_4, 0.1 M in distilled water) was used as the electrolyte. As a source of incident light, medium pressure 100W mercury lamp (HBO 100, Oriel) was used. Electrochemical response of layers on incident light during cyclic voltammetry was studied by a potentiostat (NuVant EZstat Pro with IES) [28]. The aperture between the light source and the electrodes allowed light/dark operation. The material studied was deposited on a flat titanium electrode with working area about 2 cm^2. The samples were deposited from a ultrasound dispersed powder material in water onto the electrode, immersed in the dispersion overnight.

The Cyclic Voltammetry (CV) was measured applying a potential between −0.6 and 1.2 V on working electrode against a standard saturated Ag/AgCl electrode with constant scanning speed 50 mV/s. Ten cycles were monitored to evaluate stability of the photoperiods, reproducibility and stability of deposited layers.

Results and discussion

Figure 1 shows the powder X-ray diffraction patterns of the as-prepared solid samples 1D TiO/500, 1D TiO/650, 1D TiO/800, and 1D TiO/950 as well as the intermediate amorphous precursor 1D TiO. The observation of 2θ values at 18.5° and 42.64° can be attributed to the Mylar foil, which was used as a sample holder. The fast ice-frozen precursor 1D TiO is identified as a strictly amorphous material (1D TiO). The XRD pattern of sample 1D TiO/500 annealed at 500 °C corresponds to the tetragonal anatase phase (ICDD PDF 21-1272). We observe an increase in the intensity of the anatase peaks (sample 1D TiO/650) up to an annealing temperature of 800 °C (sample 1D TiO/800). The thermal treatment of the amorphous precursor 1D TiO led to a spontaneous crystallization and controlled the anatase-rutile transformation. Sample 1D TiO/950 contains 87 % rutile phase (ICDD PDF 21-1276). The average sizes of anatase and rutile crystallites were calculated using the Scherrer equation; the continuous growth in crystallite size was determined for all heat-treated samples. The lattice parameters were also calculated, and their values are presented in Table 1. We observe that the lattice parameter *a* decreases since lattice parameter *c* increases due to the possible distortion and strain induced in the TiO_2 lattice during annealing. It can be suggested that both apical (Ti–O–Ti) and equatorial (O–Ti–O) bonds in the TiO_6 octahedron primitive cell change, and a misbalance in the electron charge density in Ti–O bonds can develop by introducing oxygen vacancies into their vicinity [29].

It has been previously reported that immersing the $TiOSO_4 \cdot 2H_2O$ MRs into ice-cold concentrated aqueous ammonia may, under certain conditions, convert the material into a novel TiO_2 product with the same size and shape as that of the starting precursor [24]. Figure 2a–d shows SEM images of samples 1D TiO/500, 1D TiO/650, 1D TiO/800 and 1D TiO/950. Highly ordered TiO_2 microrod (MR) arrays with an excellent crystal quality were fabricated by the SLS method. The annealing treatment (from 500 to 950 °C) of the

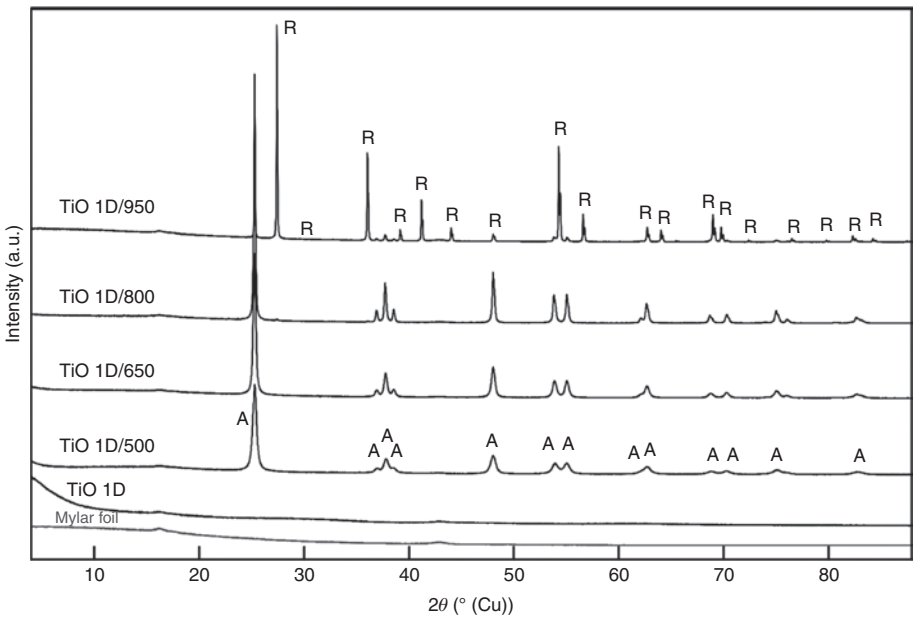

Fig. 1: X-ray diffraction patterns of the intermediate precursor 1D TiO and its post-synthesis heat treatment samples 1D TiO/500, 1D TiO/650, 1D TiO/800 and 1D TiO/950.

Table 1: Microstructural parameters obtained by XRD analysis, zeta potential and band gap of samples 1D TiO/500, 1D TiO/650, 1D TiO/800, and 1D TiO/950.

Sample	Phase composition (%)		Crystallite size (nm)		Anatase lattice parameters (Å)		Rutile lattice parameters (Å)		Zeta potential (mV)	Band gap (eV)
	Anatase	Rutile	Anatase	Rutile	a	c	a	c		
1D TiO	–	–	–	–	3.7852	9.5139	–	–	–	
1D TiO/500	100	–	18.75	–	3.7873	9.5070	–	–	−26.5	3.20
1D TiO/650	100	–	34.25	–	3.7859	9.5159	–	–	−17.8	3.19
1D TiO/800	100	–	68.74	–	3.7841	9.5233	–	–	−29.1	3.19
1D TiO/950	13	87	179.37	408.7	3.7827	9.5235	4.5929	2.9593	−38.6	2.97

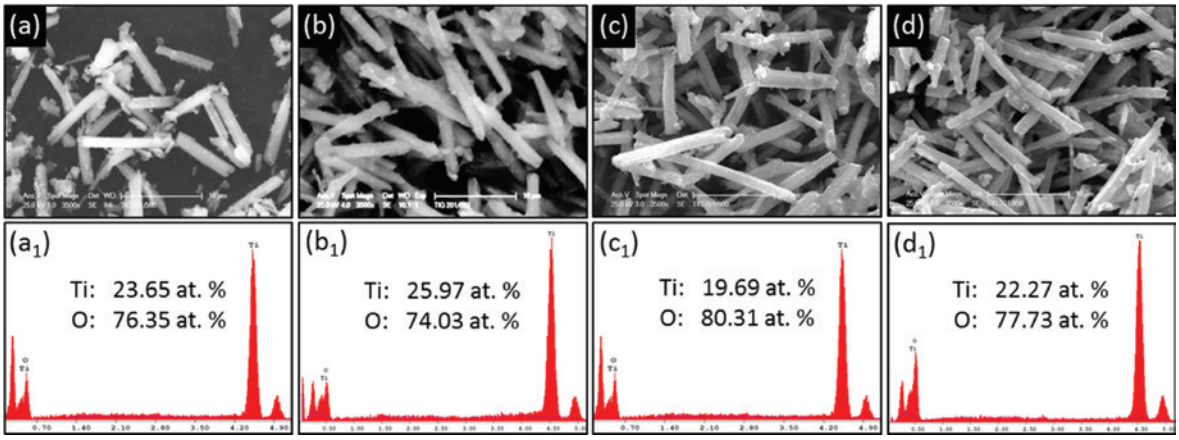

Fig. 2: SEM micrographs of (a) sample 1D TiO/500, (b) sample 1D TiO/650, (c) sample 1D TiO/800 and (d) sample 1D TiO/950 with corresponding EDS analysis (a_1–d_1) (bottom line). Insets in (a_1–d_1) are the relevant Ti/O element ratio in at. %.

intermediate precursor 1D TiO greatly improves the quality of the resultant samples, providing a decent methodology to prepare high-quality crystalline 1D TiO_2 MRs 20–25 µm in length and 2 µm in diameter. The EDS analysis confirms that samples 1D TiO/500 (Fig. $2a_1$), 1D TiO/650 (Fig. $2b_1$), 1D TiO/800 (Fig. $2c_1$) and 1D TiO/950 (Fig. $2d_1$) are very pure (no trace of SO_4^{2-} or N-residual is detected) and contain only Ti and oxygen in the ratio Ti/O = 1/3, which is typical for meta-hydroxides of titanium $[(OH_2)TiO_2]$ – sometimes called meta-titanic acid H_2TiO_3 [30, 31].

To gain a better insight into the morphological features (particle size and shape) and TiO_2 lattice spacing, the prepared 1D TiO_2 MRs were analyzed by HRTEM. Low-magnification bright-field images of samples 1D TiO/500 (Fig. 3a), 1D TiO/650 (Fig. 3b), 1D TiO/800 (Fig. 3c), and 1D TiO/950 (Fig. 3d) demonstrate similar rod-like morphologies. In the micrographs taken of samples annealed from 500 to 950 °C, at the lowest magnification (Fig. 3a–d), we observe a portion of 1D TiO_2 MRs, the structure of which is depicted at higher magnification in Fig. $3a_1$–d_1. The TiO_2 MRs consist of fine intergrowth NCs of various sizes and shapes. Furthermore, we observe a very interesting feature in the HRTEM images of samples annealed at 650 and 800 °C. The patterned surface with thin hexagonal hollowed regions (we name them nanovoids) is clearly visible, as shown in Fig. $3b_1$ (sample 1D TiO/650) and Fig. $3c_1$ (1D TiO/800). Since the nanovoids are not identified in the SEM analysis, we suggest that the nanovoids depicted by HRTEM are inside the 1D TiO_2 MRs rather than on their surface and can be regarded as internal pores [32]. At the nanometer scale, these voids have a different appearance and are seemingly regularly faceted. The interplanar spacing calculated from the high-resolution lattice fringe images (Fig. $3a_2$–c_2) is 0.352 nm, which corresponds to the (101) plane of anatase TiO_2 (JCPDS 21-1272). The SAED analysis confirms that during the annealing procedure at higher temperatures (e.g. 950 °C),

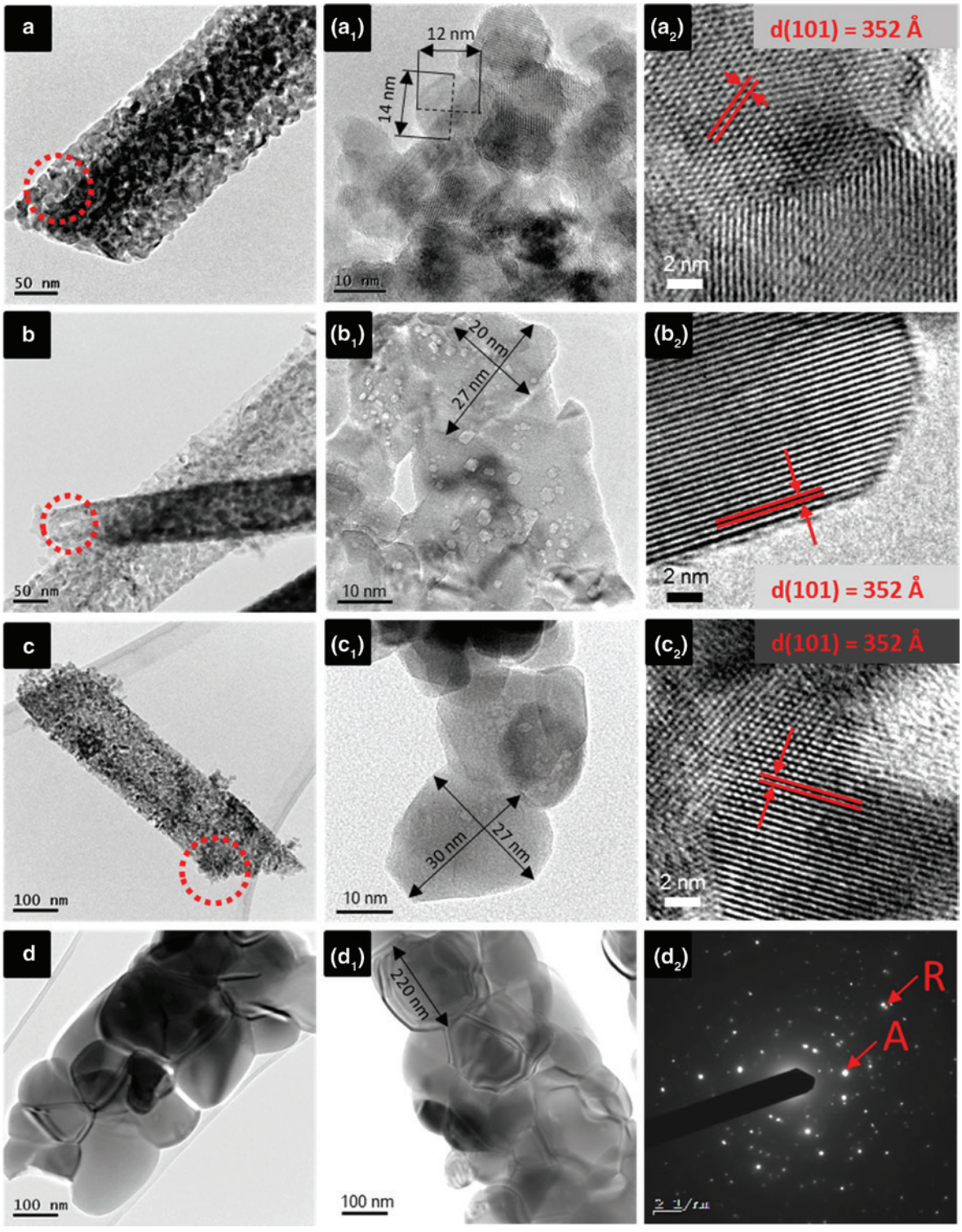

Fig. 3: Representative TEM and HRTEM images: (a–d) low magnification of samples 1D TiO/500, 1D TiO/650, 1D TiO/800, 1D TiO/950, (a_1–d_1) high magnification of the red marked area, (a_2–c_2) lattice fringes of anatase crystal lattice, (d_2) SEAD confirming anatase-rutile mixture at 950 °C.

the rutile phase begins to present as the major TiO_2 polymorph (Fig. $3d_2$), since at temperatures above 900 °C, metastable anatase transforms irreversibly into the stable rutile polymorph. This outcome corresponds well with the XRD observations (see Table 1).

Photoelectron spectroscopy was used to analyze surface stoichiometry and valence states of the 1D TiO/500, 1D TiO/650, 1D TiO/800 and 1D TiO/950 samples annealed at 500–950 °C. The surface spectrum reveals only titanium, oxygen and carbon in the superficial layers. No other elements are detected upon analyzing the surface survey spectra collected in a range of 0–1000 eV with an incremental step of 0.2 eV. The narrow scans of Ti 2p, O 1s, N 1s, S 2p and C 1s regions were then collected at a higher resolution, and the spectra were analyzed. The as-received samples are found to contain only $Ti^{(4+)}$ at the surface (458.6 and 464.5 eV). The peak separation between the Ti $2p_{1/2}$ and Ti $2p_{3/2}$ signals is 5.9 eV, which is a value typical for titanium dioxide. After argon ion sputtering, the Ti 2p lines broaden due to the removal of surface TiO_2, and new bands proving lower oxidation states are observed. After the Shirley background subtraction and the deconvolution, the spectra give rise to four components, as shown in Fig. 4a. The most intense Ti $2p_{3/2}$ band is ascribed to $Ti^{(4+)}$, but lower binding energy features are recognized as $Ti^{(3+)}$ contributions in nonstoichiometric oxides (457.1 and 456.2 eV), while the lowest binding energy of 455.0 eV is typical for $Ti^{(2+)}$. The O 1s region presented in Fig. 4b contains bands from titanium oxides, and this contribution is fitted by a broader band centered at approximately 530.0 eV. Higher binding energy bands come from hydroxyl groups bonded to titanium atoms (531.5 eV), from carbon moieties (carbonyl and carboxyl groups) and adsorbed water.

The detailed examination of the N 1s and S 2p regions reveals no presence of nitrogen and sulfur in the as-prepared and sputtered samples. Therefore, both NH_4OH, used for the hydrolysis of titanyl sulfate, and sulfate anions were completely washed off, and no nitrogen or sulfur residual is observed in the samples. The results corroborate the EDS analysis.

The SAXS analysis was applied to investigate the nanotexture of the 1D TiO_2 MRs. The scattering curve of the 1D TiO/500 sample (Fig. 5a) appears straight at a first sight. We consider that the pores are not present in this sample or their sizes are beyond the limits of our experimental setup. It seems that the sample is barely modified by the applied temperature and thus can be considered as a reference. We decided to obtain at least

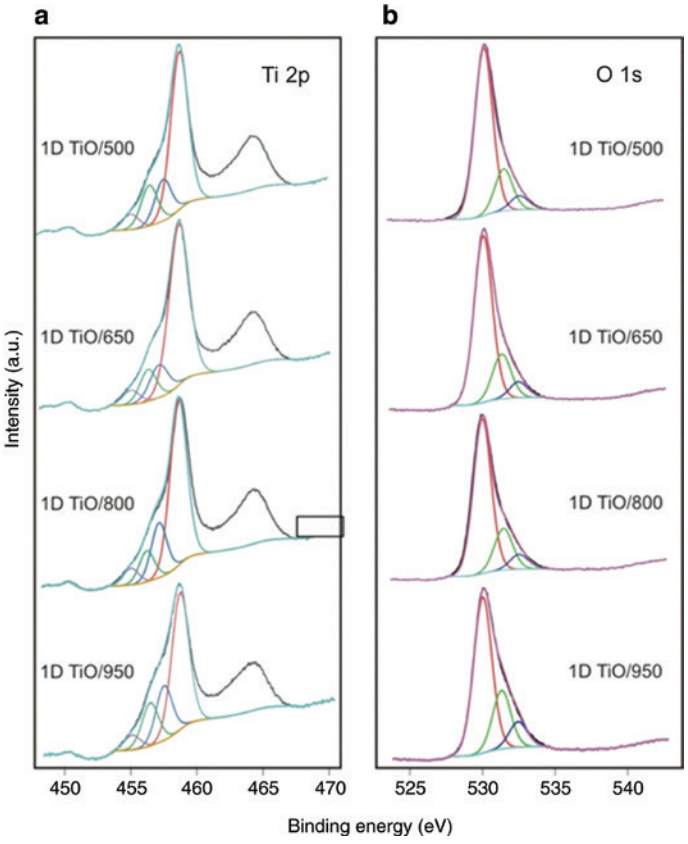

Fig. 4: XPS spectra (a) Ti 2p and (b) O 1s XP spectra of the samples 1D TiO/500, 1D TiO/650, 1D TiO/800 and 1D TiO/950.

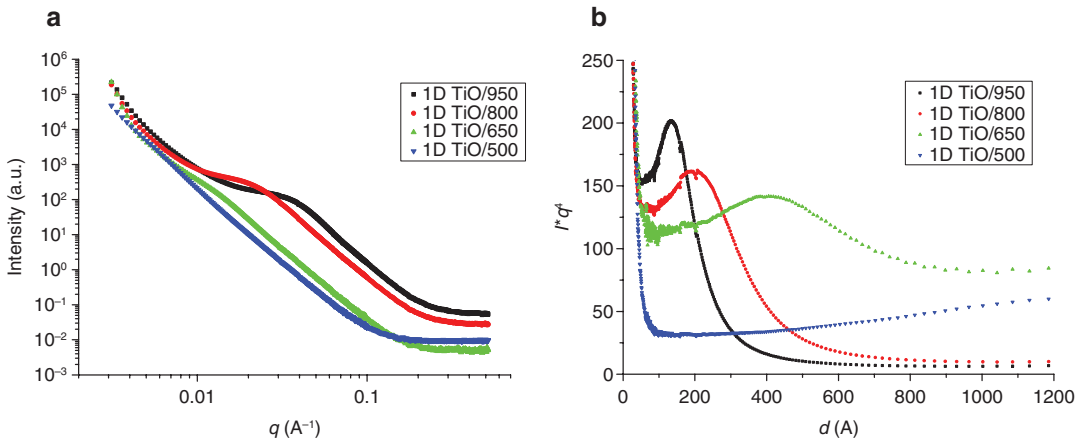

Fig. 5: (a) Small-angle X-ray scattering profiles for the samples: 1D TiO/950 (black squares), 1D TiO/800 (red circles), 1D TiO/650 (green up triangles), 1D TiO/500 (blue down triangles). (b) Normalized SAXS intensities as a function of basal spacing.

the slope of the intensity for the reference sample. In the whole measured q-region, the slope of the curve remains the same and is equal to ~4. Samples 1D TiO/650, 1D TiO/800, and 1D TiO/950 exhibit a very pronounced feature in the middle of the q-range (Fig. 5a). To estimate the sizes of the corresponding structures, the intensity was normalized by the slope obtained from the sample 1D TiO/500. This correction should give a straight line in the case of absent features. For clarity, the scattering vector q was recalculated into distances using equation $d = 2^{\star}\pi/q$. We applied these manipulations to all the curves (Fig. 5b). For sample 1D TiO/500, a small increase at higher distances is still observed, indicating the possible presence of a broad distribution of very large pores. The smallest sizes and the narrowest distribution are obtained for sample 1D TiO/950; the sizes range from 55 Å up to 400 Å, with the maximum at 135 Å. For the sample 1D TiO/800, we obtain values of 88–650 Å, with the maximum at approximately 197 Å. The broadest size distribution is obtained for sample 1D TiO/650, where we obtain a mean value of approximately 400 Å from values of 105–780 Å. Taking into consideration our results obtained by the DTA analysis, we can suggest that empty nanotunnels form after the release of confined water [33]. The fitting of the results obtained with SASFit software gives a parameter D of ~3.88, which is related to the smoothness of the surface. Usually, a calculated value of ~3 represents a 3D structure. Since the maximum dimensionality for D is approximately 4, it can be assumed that the surface of 1D TiO_2 MRs heated from 650 to 800 °C is not perfectly smooth due to the self-assembled densely packed 3D nanovoids.

To understand the thermal decomposition of the 1D TiO intermediate sample, the thermogravimetric analysis was performed (Fig. S1). One can see four reaction steps with a total mass loss of approx. 30 %. The first step might be that of weakly bonded ammonium closer to the surface, which evolves together with water up to 200–250 °C. The next step occurs at temperatures up to 500 °C, evidencing that ammonium located in the internal nanopores (nanotunnels) of the TiO_2 structure is fully eliminated [34]. In addition to the endothermic peak at 80–90 °C, assigned to the first evolution of water, two other broad peaks are observed between 200 and 500 °C, in agreement with a previous report [35]. Therefore, we can accept that the first step in the weight loss occurs at a temperature of approximately 200 °C; around this temperature, the internal pores start to empty, and previous structures begin to transform into the final tetragonal anatase. According to the HRTEM study, it is exactly above this temperature when nanovoids appear on the surface of the TiO_2 NCs. This correlation is also consistent with the fact that 1D TiO/500 does not show voids or irregular features on its surface, corresponding well with the SAXS results.

Infrared spectra of the samples are presented in Fig. S2. The Ti–O vibrations of both anatase and rutile are visible at 750 cm^{-1}. The as-prepared intermediate sample 1D TiO and heated samples 1D TiO/500, 1D TiO/650, 1D TiO/800 and 1D TiO/950 show adsorbed water, visible as a band centered at 1630–1645 cm^{-1} (deformation vibration) and a broad feature above 3000 cm^{-1} (stretching vibration). The bands are strongest in the 1D TiO

sample, and in the annealed samples, the vibrations are weaker due to the efficient desorption of water at elevated temperatures [36]. The band at 1398 cm^{-1} is very intense in the intermediate sample 1D TiO, and it is typical for carbonates formed by naturally occurring CO_2 adsorbed on alkaline surfaces. During annealing, carbonates decompose, and the corresponding band becomes very weak.

The Raman spectra, collected by a micro-Raman technique, show the presence of anatase TiO_2 (Fig. 6) in samples heated to 500–800 °C, as proven by the typical bands centered between 142 and 639 cm^{-1}. The FWHM of the E_g band centered at approximately 142 cm^{-1} is dependent on the size of crystallites, and this parameter has values of 25, 22 and 21 cm^{-1} for samples 1D TiO 500, 650 and 800, respectively, which confirm the increase in crystallite size of the samples with the annealing temperatures. At the highest temperature (950 °C), the spectrum proves the presence of rutile as the major crystalline form, which is in accordance with XRD results (see Table 1) and those of HRTEM/SAED. Due to the considerably weak cross-section of the rutile form in comparison with that of anatase at the excitation wavelength of the visible laser beam, both major rutile and minor anatase forms are represented by bands (609 cm^{-1}/A_{1g} and 446 cm^{-1}/E_g for rutile and 142 cm^{-1}/E_g for anatase) with similar intensities.

Photoelectrochemical properties of 1D TiO_2 MRs with stacked 3D nanovoids

The samples crystallized at temperatures of 500–950 °C were dispersed in deionized water, and the mixtures were stirred in an ultrasound bath. To evaluate the stability of the dispersions, the zeta potential (ζ-potential) was measured. The results show ζ-potentials in the range of –17.8 to –29.1 mV (Table 1) for anatase samples (1D TiO/500–1D TiO/800) and at –38.6 mV for the rutile sample (1D TiO/950). As general dividing line between stable and unstable dispersions is usually taken as ±30 mV, the rutile dispersion is considered completely stable. Sample 1D TiO/800 has the ζ-potential –29.1 mV, which is a value close to the stability limit, and the dispersion was observed to be highly stable as well. Samples 1D TiO/500 and 1D TiO/650 °C with ζ-potentials values –26.5 and –17.8 mV, respectively are regarded as unstable in aqueous suspension. Probably, the aggregation behavior of anatase NCs with size less than 50 nm resulting in the destabilization of the 1D TiO2 structure (see Table 1).

CV is regarded to be the best technique for acquiring qualitative information about electrochemical reactions. The stability of the electrode/electrolyte systems was tested in this study by observing the linear change in potential inserted between the working and counter (platinum) electrodes. The titanium working

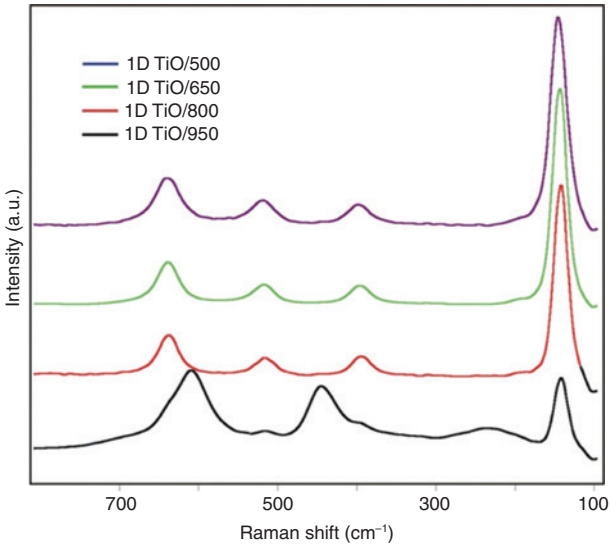

Fig. 6: Raman spectra of the annealed samples 1D TiO/500, 1D TiO/650, 1D TiO/800 and 1D TiO/950.

electrode covered by a sample deposited on its surface was placed into a three-compartment cell equipped with standard saturated Ag/AgCl and platinum counter electrodes. The current vs. potential dependencies were measured repeatedly in the dark and under irradiation by a medium-pressure mercury lamp. The geometry was set to irradiate an area of approximately 2 cm^2.

The CV was measured by applying a potential between −0.6 and 1.2 V to the working electrode (against a standard saturated Ag/AgCl electrode) with a constant scanning speed of 50 mV/s for ten cycles in light/dark operation. This study made it possible to compare the activities of the deposited layers on the electrolyte and external light perturbation. The study was conducted with five samples (the intermediate precursor 1D TiO and annealed samples 1D TiO /500, 1D TiO/650, 1D TiO/800 and 1D TiO/950) repeatedly to monitor the stability of the photoperiod, reproducibility and stability of the deposited layer.

These measurements prove the distinctive behavior of the samples to light, in which all layers reacted immediately and reproducibly to the illumination. The highest response of electric current under irradiation is obtained for the sample 1D TiO/800 (Fig. 7), showing a maximum current density exceeding 100 μA/cm^2 [37]. This value proves that water molecules are not efficiently split but indicates the possibilities of applying titanium dioxide in electrochemistry as the working electrode. Considerable resistance between the layer and the surface of the titanium electrode exists. The prepared layers are stable at high voltages (against a standard saturated Ag/AgCl electrode) and can be used for different electrochemical applications.

Plausible formation mechanism of nanovoids inside aligned 1D-TiO_2 MRs

As we mention in our results and discussion section, immersing the $TiOSO_4 \cdot 2H_2O$ into ice-cold concentrated aqueous ammonia results in the formation of novel TiO_2 MRs with the same size and shape as those of the starting precursor (Fig. 8a). This process allows for the extraction of the sulfate ions SO_4^{2-} from the $TiOSO_4$ crystals and for their subsequent replacement with the OH^- group [24]. Figure 8b shows a high-magnification TEM image of TiO_2 NCs, and the inset is the electron diffraction pattern taken from the whole TiO_2 MR obtained by using the reported SLS method. The main steps of the reaction mechanism can be described by the following reactions [38]:

$$TiOSO_4 + 2H_2O \xrightarrow{\text{Hydrolysis}} H_2TiO_3 + H_2SO_4 \quad (3)$$

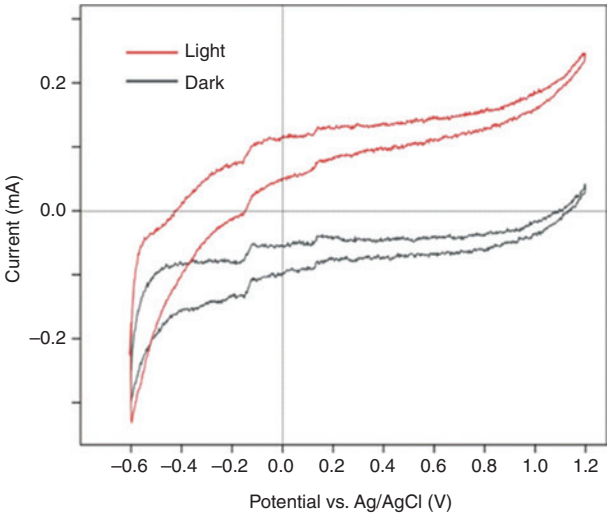

Fig. 7: Photoelectrochemical characteristics of the 1D TiO/800. The typical voltammetry measurements in dark and under irradiation are presented.

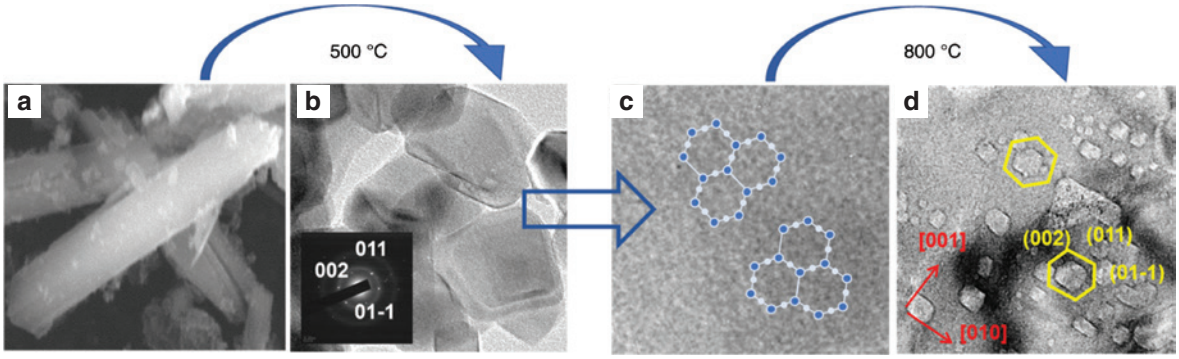

Fig. 8: Formation mechanism of nanovoids (a) low magnification of 1D TiO_2 MRs (b) single anatase TiO_2 NCs with SAED as inset, (c) evaporation of ice (water) molecules, (d) pattering of TiO_2 NC with hexagonal nanovoids viewed along [100] direction.

$$TiOSO_4 + 2NH_4OH \rightarrow H_2TiO_3 + (NH_4)_2SO_4 \tag{4}$$

$$(NH_4)_2SO_4 \xrightarrow{T\,^\circ C} NH_4HSO_4 + NH_3 \tag{5}$$

$$H_2TiO_3 \xrightarrow{T\,^\circ C} TiO_2 + H_2O \tag{6}$$

It is well known that ice is made from water, where H_2O molecules are bent and yield positively and negatively charged ends. Water molecules condense onto the surface of TiO_2 particles, and when they become sufficiently cold to freeze at 0 °C, they gather tighter to form hexagonal shapes (six-fold lattice formation) [39]. As water crystals form, the reaction temperature begins to influence the shape they become. By applying a suitable heat treatment, the water molecules depart from the 1D TiO_2 MRs (Fig. 8c), and crystals adopt the empty spaces. The ice (water) leave behind a track on the TiO_2 nanocrystals with the (101) face exposed and straight edges on the facets. The TiO_2 structure begins to change when the temperature rises from 500 to 800 °C. The heating process changes the morphology of the nanovoids, which appear as merged rectangles in the case of sample 1D TiO/650 (Fig. $3b_1$) and hexagons in the case of sample 1D TiO/800 (Fig. 8d). A high-magnification TEM image of a single TiO_2 NC containing many hexagonal nanovoids viewed along the [100] direction is presented in Fig. 8d. The boundary planes are the $[0\bar{1}1]$ [100] and [001], which are all low-index planes of the anatase crystal and exhibit the lowest surface energy formation [22].

We suggest that due to the insulating effect of the overlying amorphous sheet, the ice core does not melt during the annealing up to 500 °C (even though the hollow regions may contain ice/water). However, with increasing temperature, the amorphous sheet reduces due to transformation of the amorphous intermediate (1D TiO precursor) to anatase, and the ice core, exposed to higher temperatures, begins to melt. Therefore, the pattering of 1D TiO_2 MRs is morphologically quite different due to the different behavior of TiO_2 NCs and its dependence on the temperature.

Conclusions

In this work, the SLS method was developed by employing $TiOSO_4 \cdot 2H_2O$ as a precursor to prepare nanostructured 1D TiO_2 MRs. We investigated the dynamics of water nanoconfined in as-prepared 1D TiO_2 nanostructured MRs. The heat treatment process (from 500 to 950 °C) causes the evaporation of nanoconfined water, which leaves empty spaces (large enough to accommodate water molecules) inside the 1D TiO_2 MRs.

The self-assembled nanovoids along certain crystallographic directions of anatase NCs are confirmed by the HRTEM study. The nanovoids range in size from 5 to 78 nm for both length and width, with a depth of approximately 3.88 nm, and are responsible for the potential of applying 1D TiO_2 to photoelectrochemistry as a stable working electrode. The incorporation of the SLS method with other processes, such as doping and metal loading, can provide a promising future for 1D TiO_2 MRs as applied in PEC systems.

Acknowledgments: This work was supported by the Czech Science Foundation (Project/GACR 18-15613S). The authors gratefully acknowledge the great technical assistance (DTA and FTIR experiments) rendered by Jitka Bezdickova (IIC CAS). The authors gratefully acknowledge both reviewers for their very constructive recommendations.

References

[1] K. Zhu, N. R. Neale, A. Miedaner, A. J. Frank. *Nano Lett*. **7**, 69 (2007).
[2] Y. Ohsaki, N. Masaki, T. Kitamura, Y. Wada, T. Okamoto, T. Sekino, K. Niihara, S. Yanagida. *Phys. Chem. Chem. Phys*. **7**, 4157 (2005).
[3] J. M. Buriak, C. Toro, K. Choi. *Chem. Mater*. **30**, 7325 (2018).
[4] W. U. Huynh, J. J. Dittmer, A. P. Alivisatos. *Science* **295**, 2425 (2002).
[5] A. Fujishina, K. Honda. *Nature* **238**, 37 (1972).
[6] A. J. Nozik. *Ann. Rev. Phys. Chem*. **29**, 189 (1978).
[7] I. S. Cho, M. Logar, C. H. Lee, L. Cai, F. B. Prinz, X. Zheng. *Nano Lett*. **14**, 24 (2014).
[8] R. Daghrir, P. Drogui, D. Robert. *Ind. Eng. Chem. Res*. **52**, 3581 (2013).
[9] A. L. Linsebigler, G. Lu, J. T. Yates. *Chem. Rev.* **95**, 735 (1995).
[10] Y. J. Hwang, C. Hahn, B. Liu, P. Yang. *ACS Nano* **6**, 5060 (2012).
[11] N. Liu, C. Schneider, D. Freitag, M. Hartmann, U. Venkatesan, J. Müller, E. Spiecker, P. Schmuki. *Nano Lett*. **14**, 3309 (2014).
[12] Y. C. Pu, Y. Ling, K. D. Chang, C. M. Liu, J. Z. Zhang, Y. J. Hsu, Y. Li. *J. Phys. Chem. C* **118**, 15086 (2014).
[13] N. Fu, W. Yugi, J. Zhiliang, L. Gongxuan. *Langmuir* **26**, 447 (2010).
[14] Z. H. Zhang, P. Wang. *Energy Environ. Sci*. **5**, 6506 (2012).
[15] K. Pan, Y. Dong, W. Zhou, Q. Pan, Y. Xie, T. Xie, G. Tian. *ACS Appl. Mater. Interfaces* **5**, 8314 (2013).
[16] X. Zhang, J. Yuan, Y. Yu, Q. Dong, Z. Xiong, H. Yu, X. Zhu, H. Shen, Y. Xie. *J. Alloys Compd*. **712**, 549 (2017).
[17] A. G. Scheuermann, J. P. Lawrence, K. W. Kemp, T. Ito, A. Walsh, C. E. D. Chidsey, P. K. Hurley, P. C. McIntyre. *Nat. Mater.* **15**, 99 (2016).
[18] J. Nowotny, T. Bak, M. K. Nowotny, L. R. Shepperd. *J. Phys. Chem. B* **110**, 18492 (2006).
[19] M. Liu, N. de Leon Snapp, H. Park. *Chem. Sci.* **2**, 80 (2011).
[20] G. Liu, H. G. Yang, J. Pan, Y. Q. Yang, G. Q. Lu, H.-M. Cheng. *Chem. Rev*. **114**, 9559 (2014).
[21] F. Ning, W. Yuqi, J. Zhiliang, L. Gongxuan. *Langmuir* **26**, 447 (2010).
[22] W. Q. Han, L. Wu, R. F. Klie, Y. Zhu. *Adv. Mater*. **19**, 2525 (2007).
[23] S. Usseglio, A. Damin, D. Scarano, S. Bordiga, A. Zecchina, C. Lamberti. *J. Am. Chem. Soc*. **129**, 2822 (2007).
[24] M. Klementová, J. Bohaćek, J. Kupčík, L. Palatinus, E. Plizingrova, L. Szatmary, J. Šubrt. *Cryst. Growth* **17**, 6762 (2017).
[25] JCPDS PDF-4 database. *International Centre for Diffraction Data*, Newtown Square, PA, USA, release (2015).
[26] P. Scherrer. *Nachr. Ges. Wiss. Goettingen Math.-Phys. Kl.* **2**, 98 (1918).
[27] J. L. Labar. *Ultramicroscopy* **103**, 237 (2005).
[28] P. Dytrych, V. Drinek, J. Bumba, F. Kastanek, O. Solcova. *Int. J. Hydrog. Energy Surf.* **43**, 18136 (2018).
[29] Y. Sun, S. Sun, X. Liao, J. Wen, G. Yin, X. Pu, Y. Yao, Z. Huang. *Appl. Surf. Sci*. **440**, 440 (2018).
[30] U. Gesenhues. *Chem. Eng. Technol*. **24**, 685 (2001).
[31] T. A. Denisova, L. G. Maksimova, E. V. Polyakov, N. A. Zhuravlev, S. A. Kovyazina, O. N. Leonidova, D. F. Khabibulin, E. I. Yur'eva. *Russ. J. Inorg. Chem*. **51**, 691 (2006).
[32] L. Ren, Y. Li, J. Hou, X. Zhao, C. Pan, *ACS Appl. Mater. Interfaces* **6**, 1608 (2014).
[33] Y. Melnichenko. *Small-Angle Scattering from Confined and Interfacial Fluids*, Springer International Publishing, Switzerland (2016), eBook, ISBN 978-3-319-01104-2.
[34] E. Garcia-Gonzalez, M. D. Soriano, E. Urones-Garrote, J. M. Lopez Nieto. *Dalton Trans*. **43**, 14644 (2014).
[35] I. M. Szilagyi, J. Madarasz, G. Pokol, P. Kiraly, G. Tarkanyi, S. Saukko, J. Mizsei, A. L. Toth, A. Szabo, K. Varga-Josepovitso. *Chem. Mater*. **20**, 4116 (2008).
[36] L. Matejova, Z. Matej, R. Fajgar, T. Cajthaml, O. Solcova. *Mater. Res. Bull.* **47**, 3573 (2012).
[37] M. Mozorova, P. Dytrych, L. Spacilova, O. Soucova. *Res. Chem. Intermed.* **41**, 9307 (2015).

[38] P. M. English. *Structural Studies of Titanyl and Zirconyl Sulphate Hydrates*, Curtin University of Technology, Bentley, WA, Australia (2001). https://espace.curtin.edu.au.
[39] L. Vardiman. *Acts & Facts* **36**, 10 (2007).

Supplementary Material: The online version of this article offers supplementary material (https://doi.org/10.1515/pac-2018-1116).